

Self-assembled nanoparticle deposits formed at the contact line of evaporating micrometer-size droplets

Leonid V. Govor,^{1,*} Günter Reiter,² Jürgen Parisi,¹ and Gottfried H. Bauer¹

¹*Institute of Physics, University of Oldenburg, D-26111 Oldenburg, Germany*

²*Institut de Chimie des Surfaces et Interfaces, CNRS-UHA, 68057 Mulhouse Cedex, France*

(Received 16 December 2003; published 14 June 2004)

We report on the formation of self-assembled rings of CoPt₃ nanoparticles (ring diameter ranging from 0.6 to 1.5 μm , particle diameter 6 nm) formed in an evaporating thin film. The latter was achieved on the surface of water by spreading a binary mixture composed of two solutions: nitrocellulose dissolved in amyl acetate and CoPt₃ particles stabilized by hexadecylamine dissolved in hexane. The self-assembly process of the nanometer-sized particles into micrometer-sized rings results from phase separation in a thin film of the mixed solutions, leading to a bilayer, and the subsequent decomposition during solvent evaporation of the top hexadecylamine-rich layer into droplets. Finally, the evaporation of the remaining solvent from these droplets gives rise to a retraction of their contact line. The CoPt₃ particles located at the contact line follow its motion and self-assemble along this line.

DOI: 10.1103/PhysRevE.69.061609

PACS number(s): 81.15.-z, 47.54.+r, 47.55.Dz, 82.60.Lf

I. INTRODUCTION

Self-assembled nanoparticle structures have gained increasing interest in the last few years, and they can be produced by using different self-assembling processes which involve a variety of forces. Recently, several papers have reported the formation of nanoparticles to ringlike structures. Ohara and Gelbart [1] describe such patterning which self-assembles from a solution of nanometer-sized metal particles on a solid substrate. Rings having a diameter of 0.1–1 μm were formed during the drying process and resulted from holes nucleating in wetting thin liquid films that contain the particles. Kurikka *et al.* [2] have observed that barium ferrite nanoparticles can combine to the well-known structure of the Olympic rings (intersection of rings, ring diameter 0.6–5 μm). The mechanism of ring building was explained in terms of the formation of holes in an evaporating thin film and interparticle dipolar forces. Maillad *et al.* [3,4] found that the formation of rings of nanoparticles (silver, copper, cobalt, silver sulfide) in the micrometer range is related to Benard-Marangoni instabilities in deposited liquid films. Tripp *et al.* [5] have shown that Co nanoparticles can self-assemble in similar rings as a consequence of the following processes: dipole-directed self-assembly (typically 5–12 particles, ring diameter between 50 and 100 nm) and evaporation-driven hole formation in viscous wetting layers (ring diameter ranging from 0.5 to 10 μm). Wyrwa *et al.* [6] have described one-dimensional arrangements of metal nanoparticles formed by self-assembly processes at the phase boundary between water and dichloromethane.

In the present work, we introduce experimental evidence of how phase separation in a thin film of a binary mixture of solutions that includes a polymer and CoPt₃ nanoparticles with a stabilizer, giving rise to a bilayer structure and a sub-

sequent decomposition of the top layer into micrometer-sized droplets, can lead to the self-organized formation of rings of nanoparticles (ring diameter ranging from 0.6 to 1.5 μm , particle diameter 6 nm). As an underlying physical mechanism, we propose a self-assembly process of the nanoparticles at the droplet contact line as a consequence of the shrinking of the droplet during evaporation, i.e., the particles located at the contact line follow its motion. Our study may extend the class of self-assembling processes which involve a variety of forces governing the formation of ring structures with micrometer size [1–6].

II. EXPERIMENT

For performing our experiments, we have used a blend (B) that contains 50% of a 1% nitrocellulose solution (NC) in amyl acetate and 50% of a solution of CoPt₃ particles stabilized with hexadecylamine (HDA) and dissolved in hexane. The CoPt₃ particles with a diameter of 6 nm were prepared via the simultaneous reduction of Pt(acac)₂ and thermal decomposition of Co₂(CO)₈ in the presence of 1-adamantanecarboxylic acid and HDA both functioning as stabilizing and size-regulating agents [7]. As-prepared CoPt₃ particles were thoroughly washed in ethanol. Repeated cleaning processes make the CoPt₃ particles insoluble in either nonpolar or polar solvents due to the removal of the surfactants from the surface of the nanoparticles. Addition of HDA (7 mg/ml) to a suspension of CoPt₃ particles in hexane (17 mg/ml) leads to the formation of a clear stable colloidal solution of particles.

The thin film that provided the basis for the droplet formation was prepared by spreading a binary mixture of the solutions on a water surface in a Petri dish of 90 mm diameter [8,9]. Total spreading of a drop of the blend solution B on the water surface is obtained, due to the positive spreading coefficient [10], $S_{B/W} = \gamma_{W/A} - \gamma_{B/A} - \gamma_{B/W} = 25.3 \text{ mN/m}$. Here, $\gamma_{W/A} = 72.5 \text{ mN/m}$, $\gamma_{B/A} = 22.8 \text{ mN/m}$, and $\gamma_{B/W}$

*Author to whom correspondence should be addressed. Email address: leonid.govor@uni-oldenburg.de

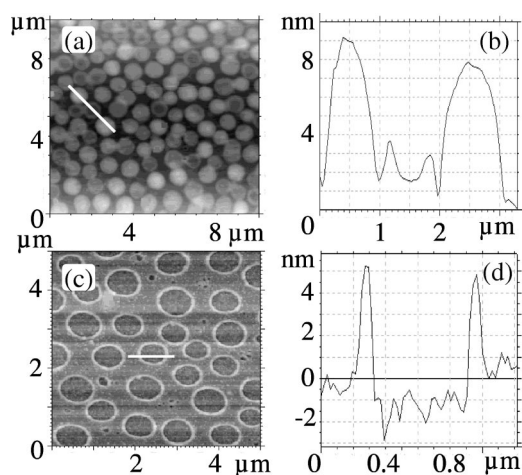


FIG. 1. (a) AFM image of HDA droplets on a cellulose film with average diameter $D_d=5.0$ nm and average height $h_d=5.0$ nm. (b) AFM profile of the scan line indicated in (a). (c) AFM image of the cellulose layer after removal of the HDA droplets. (d) Profile of the scan line indicated in (c).

$=24.4$ mN/m give the surface tension at the interfaces between water and air (W/A), between blend and air (B/A), and between blend solution and water (B/W), respectively. The interfacial tension $\gamma_{B/W}$ was derived from the difference between the surface tension of water saturated with the polymer solution and that of the polymer solution saturated with water. The values of the surface tensions were determined using a stalagmometer [11]. Since the volume of the spread drop was $3 \mu\text{l}$, the total thickness of the resulting spread fluid layer (with a diameter of 90 mm) can be estimated to be about 600 nm. After evaporation of amyl acetate and hexane, the dry thin film was transferred onto a glass substrate. The topography of these solid thin films was analyzed by atomic force microscopy (AFM, model Burleigh Vista 100) and the arrangement of the CoPt_3 particles by transmission electron microscopy (TEM, model Zeiss EM 902).

III. EXPERIMENTAL RESULTS

The AFM investigation showed that a sea-island-like phase-separated structure of hexadecylamine islands containing CoPt_3 particles (hereafter called HDA droplets) on the cellulose thin film could be found. The size of the HDA droplets depends on the place along the radius of the spreading area, but the thickness of the cellulose film was more or less constant over the full spreading area. The areas with equal HDA droplet size represented circular regions with width 2–4 mm, located symmetrically in the spreading center. In the center of the spreading area, we observed the smallest HDA droplets with height $h_d=5$ nm and diameter $D_d=650$ nm. In the circular region that was at a distance of 20 mm from the spreading center, we found the largest HDA droplets with $h_d=23.5$ nm and $D_d=1500$ nm. All other circular regions with h_d in the range from 5 to 23.5 nm (corresponding D_d in the range from 0.65 to 1.5 μm) were located between these circular regions. In Fig. 1(a), we present an AFM image (ac mode, topography) of a typical structure

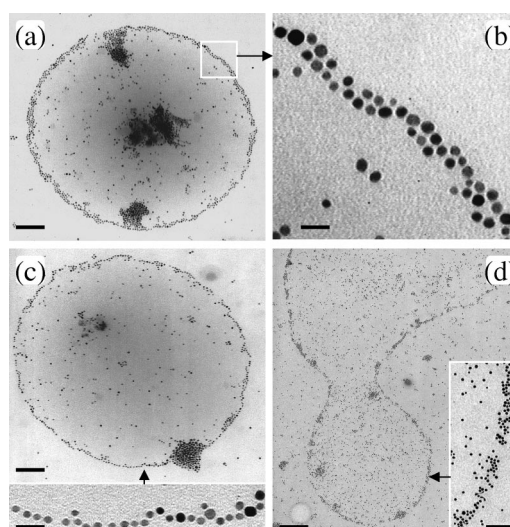


FIG. 2. TEM images of a CoPt_3 particle ring formed at the edges of HDA droplets. (a) 2D assemblage; scale bar 116 nm. (b) Magnification of the area indicated by the bright box in (a); scale bar 15 nm. (c) 1D assemblage; scale bar 98 nm. The detailed structure is magnified in the inset; scale bar 20 nm. (d) Segment of the HDA film with CoPt_3 particles assembling at its edge; scale bar 270 nm (70 nm in the inset).

of the HDA droplets with the average droplet height $h_d=5.0$ nm and the corresponding average diameter $D_d=650$ nm. The average values of both droplet height and diameter were determined from all sizes of the droplets shown in Fig. 1(a). Figure 1(b) demonstrates that some of the droplets have an M-shaped height profile.

For determination of the penetration depth of the droplets into the cellulose film, the HDA droplets were removed by immersing the specimen in hexane acting as selective solvent for HDA for a period of 5 min. Figure 1(c) shows a typical AFM picture of the remaining cellulose layer. We have measured that the thickness of the underlying cellulose film was more or less constant at about 3–4 nm. Figure 1(d) clearly illustrates that the depth of the voids that remain in the cellulose film after removal of the HDA droplets was about 1.0 nm only, indicating that the thickness of the cellulose film under the voids amounts to at least 2–3 nm. Consequently, the HDA droplets have no contact with the substrate surface, i.e., the substrate is completely covered by the cellulose film. Figure 1(d) quantifies the height of a rim that surrounds the HDA droplet to about 5 nm.

The TEM analysis of the droplet structure demonstrates that the CoPt_3 particles evidently self-assemble into a ring pattern located at the perimeter of the HDA droplets. Figures 2(a) and 2(b) display a prototypical particle ring with a diameter $D_d \approx 930$ nm. We recognize a two-dimensional (2D) ring structure. Figure 2(c) shows a particle ring with a diameter of 860 nm and a configuration which we call one dimensional (1D). In both cases, the distance between the individual particles within the ring is roughly constant. Moreover, three-dimensional (3D) particle clusters occur. We show in the spreading area only a few regions where the droplets are situated near the segments of the solid HDA film, greatly extending the droplet size. Figure 2(d) exhibits a

typical example of such a segment edge where the CoPt_3 particles assemble at the contact line. It is interesting to note that Fig. 2(d) also displays an unfinished process of droplet formation. The HDA film segments were usually considerably thicker than the height of the droplets. We emphasize that the samples shown in Figs. 2(a)–2(d) were imaged before and after removal of HDA from the samples. It turns out that both the number and position of the individual CoPt_3 particles did not change, which indicates that all particles are situated at the interface between the HDA and cellulose layers and turn out to be somewhat embedded in the cellulose layer. In other words, the CoPt_3 particles in the interior of the dry HDA droplet are located only on the interface with the cellulose layer, but not in the rest of the droplet volume. If the particles were not partially embedded in the cellulose layer, they would have been washed off during HDA removal.

IV. DISCUSSION

A. Formation of HDA droplets via phase separation

Figure 3 sketches a pictorial scenario of the mechanism we propose to be responsible for the ring formation. According to the experimental results shown in Fig. 1(c), we assume that the initial thin layer of mixed solutions on the water surface transforms into a bilayer structure which consists of a hexane-hexadecylamine-rich (HDA-rich) phase at the solution-air interface with thickness ≤ 300 nm and an amyl acetate–cellulose–rich (NC-rich) phase at the solution-water interface with thickness ≤ 300 nm [see Fig. 3(a)]. Assuming complete phase separation, the thickness of both layers may be determined from the spread drop volume, the covered area, and the volume ratio of the two phases in the initial blend solution. Note that at the beginning of evaporation the HDA-rich phase contains 99.4% hexane and only 0.6% hexadecylamine; the corresponding NC-rich phase contains 99% amyl acetate and only 1% cellulose. The number of CoPt_3 particles in each layer was about 6×10^{12} . One reason for the formation of the bilayer is that the HDA-rich phase with its lower surface free energy (18.4 mN/m for the HDA-rich component and 24.6 mN/m for the NC-rich component) wets the surface region, in order to minimize the free energy at the interface between air and solution [12–15]. The role of the CoPt_3 particles in the formation of the HDA droplet pattern was analyzed with a blend that contains 50% of a 1% NC solution in amyl acetate and 50% of a 1% HDA solution in hexane without the nanoparticles. We found that a not exactly identical, but a similar, HDA droplet pattern occurs. This means that in the HDA droplet formation the CoPt_3 particles do not play a crucial role, and in the following discussion we will not consider either the attraction between nanoparticles in the solution or that between the nanoparticles and the HDA solution.

Wetting of the HDA-rich layer on the NC-rich one takes place if the condition for the spreading coefficient $S_{\text{HDA/NC}} = \gamma_{\text{NC/A}} - \gamma_{\text{HDA/A}} - \gamma_{\text{HDA/NC}} > 0$ is satisfied. Here, $\gamma_{\text{HDA/A}}$ and $\gamma_{\text{NC/A}}$ designate the surface tension of the HDA-rich phase and that of the NC-rich phase at the boundary between the corresponding phase and air, respectively; $\gamma_{\text{HDA/NC}}$ is the sur-

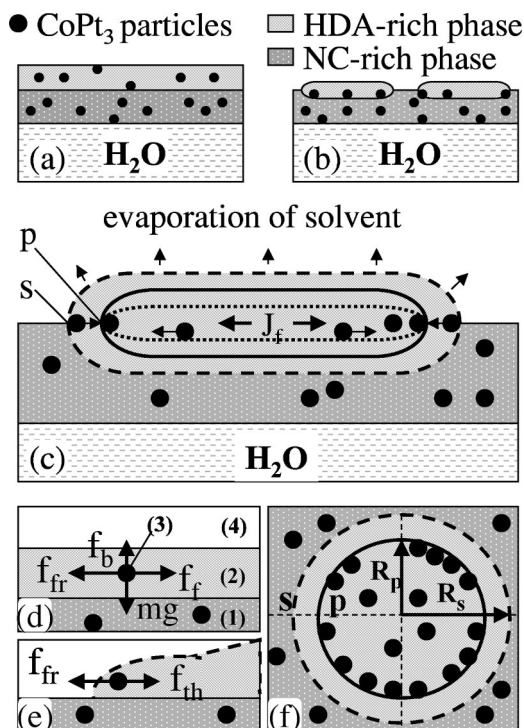


FIG. 3. Schematic illustration of the development of the phase-separated structure and the corresponding CoPt_3 particle rings. (a) Formation of phase-separated layers (bilayer structure). (b) Rupture of the HDA-rich layer into droplets. (c) Formation of the particle ring in a separated HDA-rich droplet. The contact line moves from point s to point p before it is pinned. J_r indicates the radial outward solvent flow. (d) Forces which act on the CoPt_3 particle in the interior of the HDA droplet. The media 1, 2, 3, and 4 are NC-rich layer, HDA-rich layer, CoPt_3 particle, and air, respectively. (e) Forces which act on the CoPt_3 particle located at the contact line of the HDA droplet. f_{th} is the thickening force per particle. (f) Assembling of the particles at the contact line during its motion [top view of the sketch shown in (c)].

face tension at the interface between the HDA-rich and the NC-rich phases. For a careful analysis of the evaporation process of the bilayer structure, we recorded the values of the surface tension of both HDA and NC layers in the solid state (in the following, referred to as HDAs and NCs, respectively). They were obtained from a so-called Zisman plot [16], where we measured the contact angle θ_c of the droplets (volume 1–3 μl) of water, glycerol, formamide, pyridine, cyclohexanone, decalin, and n -decane on the surface of thin HDAs and NCs films located on a glass substrate (Fig. 4). In choosing the fluids, we pursue two demands: first, a possibly large interval of surface tension for the Zisman plot and, second, the liquids must not dissolve HDAs or NCs layers. The extrapolation of the approximation lines (line 1 for the NCs film and line 2 for the HDAs film) to $\cos \theta_c = 1$ gives the critical surface tension of the film to be investigated. The term “critical” is used because any liquids taken on the Zisman plot in Fig. 4 whose surface tension enlarges the “critical surface tension” define a finite contact angle with the film investigated. The resulting values of the surface tension of both HDAs and NCs layers in the solid state amount to

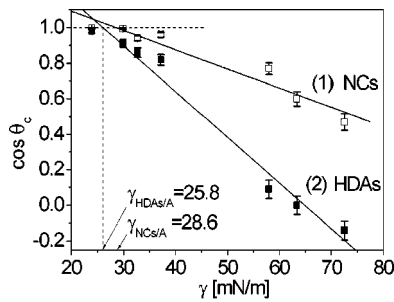


FIG. 4. Zisman plot of the NCs (fit line 1) and the HDAs films (fit line 2) measured with the liquids described in the text. The intersection of the extrapolated best-fit line with $\cos \theta_c = 1$ gives a critical surface tension of the corresponding film.

$\gamma_{\text{HDAs/A}} = 25.8 \pm 0.9$ mN/m and $\gamma_{\text{NCs/A}} = 28.6 \pm 1.2$ mN/m, respectively.

We observe $\gamma_{\text{HDAs/A}} < \gamma_{\text{NCs/A}}$ in the solid state. However, we do not know when in the course of evaporation the above relation is valid and if this inequality is applicable during the entire process. Thus, in the following, we briefly discuss the alteration of both parameters $\gamma_{\text{HDA/A}}$ and $\gamma_{\text{NC/A}}$ during evaporation. A more detailed analysis will be undertaken in a subsequent publication. First, we determined experimentally the evaporation rate of 24 ml hexane by monitoring the mass losses versus time under similar geometric and temperature conditions as for the self-assembly experiment, and we found 3.30 ± 0.06 mg/s. The analogous experimentally estimated evaporation rate of 24 ml of amyl acetate was 0.16 ± 0.01 mg/s. Second, we determined experimentally the evaporation rate of the respective solvents in a two-phase solvent that contained 24 ml hexane and 24 ml amyl acetate. In the latter case, the evaporation process is divided into two distinct regimes; first, the evaporation of hexane at 2.45 ± 0.11 mg/s and, second, that of amyl acetate at 0.13 ± 0.01 mg/s. On the one hand, we found that the evaporation rate of hexane in a two-phase solvent is 26% lower than that of pure hexane. The corresponding decrease of the evaporation rate of amyl acetate amounts to 19%. On the other hand, we observed that the evaporation rate of hexane (pure or in a two-phase solvent) is about 20 times larger than that of amyl acetate. We assume the existence of this relation between the evaporation rates of hexane and amyl acetate in our self-assembly experiment. From the data for the evaporation rate in the two-phase solvent, we have determined the time t_0 necessary to evaporate 1.0 mg hexane ($t_0 = 0.4$ s) and 1.3 mg amyl acetate ($t_0 = 10$ s) in our self-assembly experiment. With the mass loss of each solvent during the evaporation time t for $0 < t < t_0$ described as $m_s = m_{s0}(1 - t/t_0)$, where m_{s0} denotes the mass at the starting point of the evaporation process, we calculate the time dependent surface tension γ of the binary HDA solution that contains hexane ($\gamma_{s/A}$) and hexadecylamine ($\gamma_{\text{HDAs/A}}$) as [10]

$$\gamma = \gamma_{s/A}N_s + \gamma_{\text{HDAs/A}}N_{\text{HDAs}} - \beta N_s N_{\text{HDAs}}, \quad (1)$$

where β is a semiempirical constant. Here, $N_s = (1 - t/t_0)/(1 - t/t_0 + \alpha)$ and $N_{\text{HDAs}} = \alpha/(1 - t/t_0 + \alpha)$ are the fractions of the corresponding component in the binary solution, where α

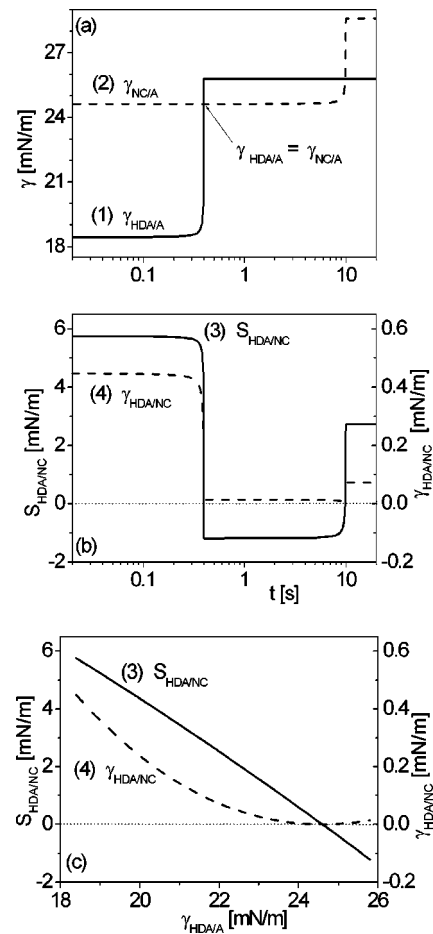


FIG. 5. (a) Calculated surface tension versus evaporation time for the HDA-rich layer (line 1) and the NC-rich layer (line 2). (b) and (c) calculated the spreading coefficient $S_{\text{HDA/NC}}$ (line 3) and that of the interfacial tension between two phases, $\gamma_{\text{HDA/NC}}$ (line 4) as a function of time and as a function of the surface tension of the HDA-rich layer, respectively.

$= m_{\text{HDAs}}/m_{s0}$, and m_{HDAs} is the mass of hexadecylamine in the top layer. Accordingly, Eq. (1) can be used for the NC-rich phase that contains amyl acetate and cellulose. Figure 5(a) displays the results calculated for both values of the surface tension versus the evaporation time. Line 1 characterizes the evaporation process of the HDA-rich layer with $\gamma_{s/A} = 18.4$ mN/m (hexane), $\gamma_{\text{HDAs/A}} = 25.8$ mN/m, $m_{s0} = 1.0$ mg, $m_{\text{HDAs}} = 4.2 \times 10^{-3}$ mg, and $\beta = 1$. Line 2 describes the evaporation of the NC-rich phase with $\gamma_{s/A} = 24.6$ mN/m (amyl acetate), $\gamma_{\text{NCs/A}} = 28.6$ mN/m, $m_{s0} = 1.3$ mg, $m_{\text{NCs}} = 7.5 \times 10^{-3}$ mg, and $\beta = 1$. The corresponding spreading coefficient $S_{\text{HDA/NC}}$ and the change of $\gamma_{\text{HDA/NC}}$ versus evaporation time are depicted by the lines 3 and 4 in Fig. 5(b). In Fig. 5(c), they are presented versus the surface tension of the HDA-rich layer. Obviously, $S_{\text{HDA/NC}}$ is positive until $\gamma_{\text{HDA/A}} = \gamma_{\text{NC/A}}$ and before dewetting of the HDA-rich layer on the surface of the NC-rich layer starts. Line 4 shows the interfacial tension at the interface between the two phases which was calculated via $\gamma_{\text{HDA/NC}} = \gamma_{\text{HDA/A}} + \gamma_{\text{NC/A}} - 2(\gamma_{\text{HDA/A}}\gamma_{\text{NC/A}})^{0.5}$ [17].

The characteristic equilibrium thickness d_e of the wetting HDA-rich layer on the NC-rich layer results from a compe-

titution between attractive long-range forces (as measured by $\gamma_{\text{HDA/A}}$ with the tendency to make the film thicker) and short-range forces (as characterized by $S_{\text{HDA/NC}}$ with the tendency to thin the film) and is determined according to [18–20]

$$d_e = a(3\gamma_{\text{HDA/A}}/2S_{\text{HDA/NC}})^{1/2}, \quad (2)$$

where $a^2 = |A|/6\pi\gamma_{\text{HDA/A}}$ is a molecular length, derived from the ratio of the effective Hamaker constant $A = A_{12} - A_{22}$ and the surface tension of the HDA-rich layer. Here, we have denoted the NC-rich layer as body 1 and the HDA-rich layer as body 2. The Hamaker constant $A_{12} = (A_{11}A_{22})^{1/2}$ [21,22] describes the dispersive interaction between NC-rich and HDA-rich layers, where A_{11} and A_{22} are the individual Hamaker constants [23] of the NC-rich and HDA-rich layers, respectively. Based on these considerations, we conclude that the HDA-rich layer cannot become thinner than d_e . If there is not enough material to cover the whole substrate with a film of thickness d_e , islands or droplets called ‘‘pancakes’’ [18–20] will be formed, all having a thickness of d_e .

As in the course of our experiment, increasingly more solvent evaporates from the film, the surface tension $\gamma_{\text{HDA/A}}$ of the upper layer rises, while the corresponding spreading coefficient $S_{\text{HDA/NC}}$ becomes smaller, Fig. 5(c). We recognize from Figs. 5(b) and 5(c) that the equilibrium thickness d_e [Eq. (2)] varies strongly with the evaporation time according to the transient of the spreading coefficient $S_{\text{HDA/NC}}$, which is caused by the variation of $\gamma_{\text{HDA/A}}$ from 18.4 to 24.6 mN/m. This alteration leads to a decrease of $S_{\text{HDA/NC}}$ by more than two orders of magnitude. For example, with $\gamma_{\text{HDA/A}} \approx 24$ mN/m and the corresponding $S_{\text{HDA/NC}} \approx 0.25$ mN/m, and further using $a = 0.3$ nm [19], we obtain an equilibrium thickness of the wetting HDA-rich layer on the NC-rich layer of about $d_e \approx 4$ nm. Here, we have assumed a to be a constant. Indeed, the molecular length $a^2 = [(A_{11}A_{22})^{1/2} - A_{22}]/6\pi\gamma_{\text{HDA/A}}$ will change on altering the Hamaker constant A_{22} and $\gamma_{\text{HDA/A}}$ during the evaporation time $0 < t \leq 0.4$ s (the change of A_{11} in this time interval is very small). The change in A_{22} is proportional to that of $\gamma_{\text{HDA/A}}$, which changes by a factor of about 1.4. In this case, the change of a will be very small and cannot influence essentially our evaluation of d_e . Based on these considerations, we expect that the equilibrium thickness d_e of the HDA-rich layer when it decomposes into droplets (or ‘‘pancakes’’) was in the range of the diameter of a CoPt_3 particle. In this case, the particles were located near the interface between the HDA-rich and the NC-rich layers. This assumption is in good agreement with our experimental result, which indicates that all nanoparticles shown in Fig. 2 were located on the cellulose layers. This argument follows from the result that both number and position of the individual CoPt_3 particles were unchanged by the removal of HDA droplets from the samples (see Sec. III).

The decay of the HDA-rich layer into droplets starts at a layer thickness $d < d_e$ and becomes significantly fast for a layer thickness about 10–15 % [1] thinner than d_e . Below this value, the HDA-rich layer gets unstable and formation and growth of dry patches occurs, in order to achieve the equilibrium thickness d_e . Consequently, under these condi-

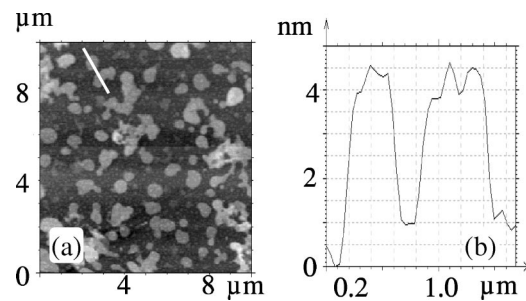


FIG. 6. (a) AFM image of HDA clusters spin coated from a 0.062% HDA solution on a cellulose film. The diameter of the clusters is about 700 nm, their heights about 3 and 6 nm, respectively. (b) Profile of the scan line indicated in (a).

tions, the layer decomposes into droplets [19,24] [see Fig. 3(b)]. In support of our model for the underlying mechanism sketched in Figs. 3(a) and 3(b), we have spin-coated an HDA film onto a glass substrate covered with a cellulose film (thickness 2–4 nm). The concentration of the HDA solution (in hexane) was varied in the range from 0.015 to 0.5 wt %. We found that, for all concentrations, HDA forms dropletlike clusters on the NC-coated substrate. The diameter and height of these clusters depend on the HDA concentration in the solution. For example, Fig. 6 visualizes the clusters that were spin-coated from the 0.062% HDA solution onto a NC film. The diameter of the clusters is about 700 nm; their height amounts to either 3 or 6 nm. These results are in good agreement with those described above for the droplet formation illustrated in Fig. 3. We emphasize that at the end of the dewetting process the resulting HDA pancakes still contain a solvent, since without solvent HDA would crystallize and the dewetting would stop before the quasiequilibrated pancakes formed a circular shape. The HDA pancakes also contain CoPt_3 particles.

B. Formation of a nanoparticle ring at the edge of an HDA droplet

Figure 3(c) presents our explanation of the drying of a pancake of the HDA-rich phase that contains CoPt_3 particles. As long as the droplet contact line (interface between air, liquid, and substrate) is not pinned, the reduction of the droplet volume by evaporation leads to a motion of its interface from the dashed to the solid line, i.e., the contact line moves from point s to point p . Those particles that are located at the contact line follow its shrinking and assemble into a ringlike pattern. The nature of the force governing such ordering can be capillary attraction arising when the particle size is comparable to the thickness of the HDA-rich pancake during dewetting [25–27]. These papers clearly demonstrate that in all experiments the 2D ordering of the particles always started when the tops of the micrometer and submicrometer particles protruded from the liquid layer. The capillary attraction energy is proportional to r^2 (r is the particle radius) and can be much larger than the thermal energy (kT) even with particles of a diameter of about 10 nm [26]. When the contact line gets pinned (point p), the droplet shape changes from the solid to the dotted line in Fig. 3(c), and an outward

flow J_f of the solvent develops, since the solvent removed via evaporation from the edge of the droplet must be replenished by a flow from the interior [28–30]. The flow J_f can transfer up to 100% of the solute to the contact line [30].

In the following, we address the correlation between the number of CoPt₃ particles which are assembled at the contact line during its motion and the number of those particles which move with the flow J_f . For a single particle with a diameter of 6 nm and covered with a 1.4 nm thick HDA shell, the gravity force is $mg=2.2 \times 10^{-20}$ N [Fig. 3(d)], and the corresponding buoyancy force in the HDA-rich layer $f_b = \rho V_p g = 2.6 \times 10^{-21}$ N. The parameters m and V_p are the mass and volume of a particle, g denotes the gravitational acceleration, and $\rho=0.79$ g/ml and $\rho=0.80$ g/ml are the densities of the HDA- and the NC-rich layer, respectively. The resulting relation $mg > f_b$ also allows that during the formation of the HDA- and NC-rich layers the CoPt₃ particles can already move downward into the water substrate. During evaporation of the solvent, the viscosity of both layers increases. If the values of the viscosity become large enough, in order to prevent the motion of the particles into the water substrate, the particles will be dispersed in both layers. For the modeling of the nanoparticle ring arrangement, our starting point consists of a homogeneous lateral distribution of the CoPt₃ particles in the solution before the droplet formation occurs. We have to admit that the number of nanoparticles we finally detect on the cellulose layer is lower than that expected from the concentration of the initial solution. For example, the expected numbers of CoPt₃ particles contained on the surface inside the rings (excluding the particles at the contact line forming the ring) for the samples shown in Figs. 2(a) and 2(c) must be about 1400 and 1200, respectively (determined from the concentration of particles in the initial blend solution). Experimentally, we counted about 540 particles for the sample shown in Fig. 2(a) and about 220 particles in the sample shown in Fig. 2(c), i.e., we have about 39% and 18% of the expected number of particles, respectively. We assume that the missing particles have dropped into the water substrate or the particles had a dissimilar distribution in the spread film.

We assume that, before the contact line gets pinned and the flow J_f sets in, the majority of the CoPt₃ particles were dispersed laterally homogeneously near or onto the cellulose layer. The possibility of their motion from the center to the contact line in a fluid HDA droplet via the solvent flow J_f can be qualitatively estimated by the equation $f_f = f_{fr}$, where other contributions are negligible compared to the flow force f_f and the friction force f_{fr} [see Fig. 3(d)]. The Reynolds coefficient for the motion of a CoPt₃ particle with the radius r_s in the flow J_f is $Re = \rho v r_s / \eta = 5.9 \times 10^{-3} v$ s/m. Here $\rho = 0.79$ g/ml, $\eta = 5.9 \times 10^{-4}$ Ns/m², and v are the density, viscosity, and velocity of the flow J_f , respectively; $r_s = r + \delta = 4.4$ nm is the radius of the CoPt₃ particle overcoated with a HDA monolayer. For example, for the velocity $v = 1$ m/s, the Reynolds coefficient amounts to $Re = 5.9 \times 10^{-3}$, and the motion of the nanoparticle in such a flow is laminar. The force f_f ,

$$f_f = 6\pi\eta r_s v, \quad (3)$$

describes the interaction of the solvent flow J_f (including the HDA molecules) with a nanoparticle. The counterforce f_{fr}

$= Kf_z$ is a lateral friction force acting on the particle, where K is a dimensionless coefficient of order unity [1] and f_z is the attractive dispersion force along the vertical z axis between each particle and the NC-rich layer. The interaction energy between a small CoPt₃ particle and the NC-rich layer can be described as $W(D) = -Ar/6D$ [17], the corresponding interaction force becomes $f_z = \partial W(D)/\partial D = Ar/6D^2$, where $r = 3$ nm is the radius of the CoPt₃ particle, D is the distance between the particle and the NC-rich layer, and A is the Hamaker constant appropriate to the CoPt₃ particle, interacting through hexadecylamine with the NC-rich layer. In our case, the thickness of the HDA layer [body 2 in Fig. 3(d)] between the CoPt₃ particle (body 3) and the NC-rich layer (body 1), as well as between the CoPt₃ particle and air (body 4), is very small. That means that all interaction components between the surrounding materials across the CoPt₃ particle will contribute to the total interaction energy between each particle and the NC-rich layer [31,32]. In this case, from standard arguments, the interaction force between the CoPt₃ particle 3 and the NC-rich layer 1 across the HDA layer 2 can be expressed by [17]

$$f_z = \frac{r}{6} \left[\frac{A_{232}}{(2r)^2} - \frac{\sqrt{A_{121}A_{323}}}{(2r + \delta)^2} - \frac{\sqrt{A_{424}A_{323}}}{(2r + \delta)^2} + \frac{\sqrt{A_{424}A_{121}}}{(2r + 2\delta)^2} \right], \quad (4)$$

where $\delta = 1.4$ nm is the thickness of the HDA monolayer adsorbed on the CoPt₃ particle. The effective Hamaker constants A_{232} , A_{121} , A_{323} , and A_{424} can be composed from the respective Hamaker constants of each medium [21,22]

$$A_{232} = A_{323} = (\sqrt{A_{22}} - \sqrt{A_{33}})^2, \quad A_{121} = (\sqrt{A_{11}} - \sqrt{A_{22}})^2, \\ A_{424} = (\sqrt{A_{44}} - \sqrt{A_{22}})^2. \quad (5)$$

The individual Hamaker constants A_{ii} can be extracted from experimentally determined data of the surface tension γ_{ii} as [17]

$$A_{ii} = 24\pi\gamma_{ii}(D_0)^2, \quad (6)$$

with a cutoff intermolecular separation $D_0 = 0.165$ nm [17]. Equation (6) yields $A_{22} = 5.3 \times 10^{-20}$ J for experimentally obtained values of $\gamma_{\text{HDA}/\text{A}} = 25.8$ mN/m taken from the Zisman plot. For the NC-rich layer with $\gamma_{\text{NC}/\text{A}} = 24.6$ mN/m at the moment of dewetting of the HDA-rich layer, the corresponding Hamaker constant is $A_{11} = 5.0 \times 10^{-20}$ J. Upon further considering the characteristic value of the Hamaker constant for most metals, $A_{33} \approx 4 \times 10^{-19}$ J [17] and $A_{44} = 0$, the effective Hamaker constants $A_{232} \approx 1.6 \times 10^{-19}$ J, $A_{121} \approx 0.4 \times 10^{-22}$ J, $A_{424} \approx 5.3 \times 10^{-20}$ J could be determined. For the above values attributed to the parameters in Eq. (4), the calculated interaction force becomes $f_z \approx 1.3 \times 10^{-12}$ N. Assuming furthermore $K \approx 0.5$ [1], the friction force is quantified as $f_{fr} \approx 6.6 \times 10^{-13}$ N. From the equation $f_f = f_{fr}$, the velocity v of the flow J_f that is necessary for the motion of the CoPt₃ particle from the interior to the contact line would be $v \approx 6.7 \times 10^3$ $\mu\text{m/s}$, which means that only at such a high velocity would the flow force be sufficiently strong to overcome the frictional forces and drag the nanoparticles. At

lower velocities, the nanoparticles do not move.

So far, no experimental studies or results are available on the flow velocity in micrometer-sized droplets with a pinned contact line on a fluid substrate. For macrosized droplets on a solid substrate, only a few studies have been published, including the approach for the extraction of the lateral flow velocity [30,33]. Deegan *et al.* [30] measured the velocity in the fluid by tracking the motion of polystyrene microspheres with a diameter of $1\ \mu\text{m}$ inside a drying water droplet with a radius of $2\ \text{mm}$, when the contact line was pinned. They found that the velocity of the water flow J_f near the contact line was about $6\ \mu\text{m/s}$. The evaporation rate in the diffusion-limited regime was proportional to the diameter of the evaporating droplet. This happens because the evaporation rate is lowered due to the finite probability that an evaporated molecule will return to the droplet [33]. In our case, where the evaporating droplet has a diameter of about $1\ \mu\text{m}$, the velocity of the flow J_f must be essentially smaller than $6\ \mu\text{m/s}$. In conclusion, the value $v \approx 6.7 \times 10^3\ \mu\text{m/s}$, claimed above to be necessary for the motion of a CoPt_3 particle from the interior to the contact line, cannot be reached in the HDA-rich droplets investigated here.

According to these results, it is not very plausible that the particles found at the perimeter of the droplet have been transferred from the interior of the droplet. Thus, we assume that practically all the CoPt_3 particles in a ring are assembled due to the retraction of the contact line caused by evaporation. This is graphically demonstrated in Figs. 3(e) and 3(f), where the dashed line represents the initial fluid droplet, immediately after the HDA-rich layer was ruptured into droplets (radius R_s), and the solid line represents the dry droplet (radius R_p). The force acting radially on the contact line, associated with a force to thicken the HDA-rich droplet (pancake), is given by [19]

$$F_{th} = 2\pi R S_{\text{HDA/NC}} [(d_e/d)^2 - 1], \quad (7)$$

where R denotes the radius of the fluid HDA-rich droplet. This thickening force F_{th} drags the CoPt_3 particles with the retraction of the droplet perimeter (the three-phase contact line), until this force is balanced by the total friction force F_{fr} . The force F_{fr} results from the superposition of the friction forces of individual nanoparticles, located at the contact line of a droplet with radius $R=R_p$, and can be formulated via the friction force per particle, $f_{fr}=Kf_z$ [see Eq. (4)],

$$F_{fr} = Kf_z \phi (R_s^2 - R_p^2)/r_s^2. \quad (8)$$

Here, ϕ denotes the area fraction covered by particles. The expected value $\phi=126 \times 10^{-3}$ was derived from the concentration of particles in the initial blend solution. Experimentally, from the concentration of particles in the interior of the rings illustrated in Figs. 2(a) and 2(c), we have found that not

all particles remained at the interface between the HDA and the cellulose layers, i.e., the experimental values of ϕ for the rings shown in Figs. 2(a) and 2(c) amount to 48×10^{-3} and 23×10^{-3} , respectively. The term $\phi(R_s^2 - R_p^2)/r_s^2$ in Eq. (8) accounts for the number of particles located between the dashed and the solid lines in Fig. 3(f). The radius R_p can be extracted from Eqs. (7) and (8) as

$$R_p = \frac{1}{2} \left\{ \left[\frac{2\pi r_s^2 S_{\text{HDA/NC}} [(d_e/d)^2 - 1]}{Kf_z \phi} \right]^2 + 4R_s^2 \right\}^{1/2} - \frac{\pi r_s^2 S_{\text{HDA/NC}} [(d_e/d)^2 - 1]}{Kf_z \phi}. \quad (9)$$

The validity of Eq. (9) can be checked with the rings shown in Figs. 2(a) and 2(c), the number $N_d=131$ of which was observed on the sample with an area $A_s=18.2 \times 21.4\ \mu\text{m}^2$. From these data, the value $R_s=(A_s/4N_d)^{0.5}=860\ \text{nm}$ is estimated. The predominant parameters in Eq. (9) are $S_{\text{HDA/NC}}$, d , and K . With $S_{\text{HDA/NC}}=0.25\ \text{mN/m}$, $d=0.85d_e$ [1], and $K=0.5$ [1], the corresponding radius R_p calculated from Eq. (9) for the ring shown in Fig. 2(c) becomes $560\ \text{nm}$ (experimentally, $430\ \text{nm}$). The corresponding value of R_p of the ring shown in Fig. 2(a), derived from Eq. (9) with $S_{\text{HDA/NC}}=0.25\ \text{mN/m}$, $d=0.85d_e$, and $K=0.5$, is $690\ \text{nm}$ (experimentally, $R_p=465\ \text{nm}$). Obviously, the above agreement between the experimentally measured and theoretically calculated values of R_p supports our model that CoPt_3 particle rings were formed by the retraction of the contact line of the HDA droplet during evaporation.

V. CONCLUSION

We have experimentally demonstrated that self-assembly of rings of CoPt_3 nanoparticles in ultrathin polymer films derives from phase separation of a binary solution on the water surface. This process leads to the formation of a bilayer structure which consists of an HDA-rich layer at the solution-air interface and a NC-rich layer at the solution-water interface. The subsequent dewetting of the HDA layer on the surface of the NC layer leads to its decomposition into micrometer-sized droplets. The simultaneous evaporation of the HDA droplets gives rise to a shrinking of their perimeter, and the CoPt_3 particles located at the contact line follow this retraction. The self-assembly of CoPt_3 particles along the contact line in ordered one- or two-dimensional rings strongly benefits from the attraction between the particles.

ACKNOWLEDGMENTS

The authors would like to thank E. Shevchenko and H. Weller for the preparation of CoPt_3 nanoparticles and for valuable discussion of experimental results.

- [1] P. C. Ohara and W. M. Gelbart, *Langmuir* **14**, 3418 (1998).
- [2] V. Kurikka, P. M. Shafi, I. Felner, Y. Mastai, and A. Gedanken, *J. Phys. Chem.* **103**, 3358 (1999).
- [3] M. Maillard, L. Motte, A. T. Ngo, and M. P. Pileni, *J. Phys. Chem.* **104**, 11 871 (2000).
- [4] M. Maillard, L. Motte, and M. P. Pileni, *Adv. Mater. (Weinheim, Ger.)* **13**, 200 (2001).
- [5] S. L. Tripp, S. V. Puszta, A. E. Ribbe, and A. Wei, *J. Am. Chem. Soc.* **124**, 7914 (2002).
- [6] D. Wyrwa, N. Beyer, and G. Schmid, *Nano Lett.* **2**, 419 (2002).
- [7] E. Shevchenko, D. Talapin, A. Kornowski, A. Rogach, and H. Weller, *J. Am. Chem. Soc.* **124**, 11 480 (2002).
- [8] L. V. Govor, I. A. Bashmakov, F. N. Kaputski, M. Pientka, and J. Parisi, *Macromol. Chem. Phys.* **201**, 2721 (2000).
- [9] L. V. Govor, I. A. Bashmakov, R. Kiebooms, V. Dyakonov, and J. Parisi, *Adv. Mater. (Weinheim, Ger.)* **13**, 588 (2001).
- [10] A. W. Adamson, *Physical Chemistry of Surfaces* (Wiley, New York, 1982).
- [11] L. V. Govor, G. H. Bauer, G. Reiter, E. Shevchenko, H. Weller, and J. Parisi, *Langmuir* **19**, 9573 (2003).
- [12] F. Bruder and R. Brenn, *Phys. Rev. Lett.* **69**, 624 (1992).
- [13] U. Steiner, J. Klein, and L. J. Fetters, *Phys. Rev. Lett.* **72**, 1498 (1994).
- [14] W. Straub, F. Bruder, R. Brenn, G. Krausch, H. Bielefeldt, A. Kirsch, O. Marti, J. Mlynek, and J. F. Marko, *Europhys. Lett.* **29**, 353 (1995).
- [15] K. Tanaka, A. Takahara, and T. Kajiyama, *Macromolecules* **29**, 3232 (1996).
- [16] W. A. Zisman, *Contact Angles, Wettability, and Adhesion*, Advanced Chemistry Series Vol. 43 (ACS, Washington, DC, 1991).
- [17] J. N. Israelachvili, *Intermolecular and Surface Forces* (Academic Press, London, 1991).
- [18] P. G. de Gennes, *Rev. Mod. Phys.* **57**, 827 (1985).
- [19] F. Brochard-Wyart and J. Daillant, *Can. J. Phys.* **68**, 1084 (1990).
- [20] F. Brochard-Wyart, J. M. di Meglio, and P. G. de Gennes, *Langmuir* **7**, 335 (1991).
- [21] J. Visser, *Adv. Colloid Interface Sci.* **3**, 331 (1972).
- [22] D. Bargeman and F. van Voorst Vader, *J. Electroanal. Chem. Interfacial Electrochem.* **37**, 45 (1972).
- [23] H. C. Hamaker, *Physica (Amsterdam)* **9**, 1058 (1937).
- [24] F. Brochard-Wyart, P. Martin, and C. Redon, *Langmuir* **9**, 3682 (1993).
- [25] N. D. Denkov, O. D. Velev, P. A. Kralchevsky, I. B. Ivanov, H. Yoshimura, and K. Nagayama, *Nature (London)* **361**, 26 (1993).
- [26] P. A. Kralchevsky, N. D. Denkov, V. N. Paunov, O. D. Velev, I. B. Ivanov, H. Yoshimura, and K. Nagayama, *J. Phys.: Condens. Matter* **6**, A395 (1994).
- [27] A. S. Dimitrov, C. D. Dushkin, H. Yoshimura, and K. Nagayama, *Langmuir* **10**, 432 (1994).
- [28] E. Adachi, A. S. Dimitrov, and K. Nagayama, *Langmuir* **11**, 1057 (1995).
- [29] R. D. Deegan, O. Bakajin, T. F. Dupont, G. Huber, S. R. Nagel, and T. A. Witten, *Nature (London)* **389**, 827 (1997).
- [30] R. D. Deegan, O. Bakajin, T. F. Dupont, G. Huber, S. R. Nagel, and T. A. Witten, *Phys. Rev. E* **62**, 756 (2000).
- [31] S. Nir and C. S. Vassiliev, in *Thin Liquid Films: Fundamentals and Applications*, edited by I. B. Ivanov (Marcel Dekker, New York, 1988), p. 207.
- [32] G. Reiter, A. Sharma, A. Casoli, M.-O. David, R. Khanna, and P. Auroy, *Langmuir* **15**, 2551 (1999).
- [33] J. T. Davies and E. K. Rideal, *Interfacial Phenomenon* (Academic Press, New York, 1963).